

Coupling Lattice Boltzmann and Molecular Dynamics models for dense fluids

A. Dupuis, E.M. Kotsalis and P. Koumoutsakos

Computational Laboratory, ETH Zurich, CH-8092, Switzerland.

June 11, 2018

Abstract

We propose a hybrid model, coupling Lattice Boltzmann and Molecular Dynamics models, for the simulation of dense fluids. Time and length scales are decoupled by using an iterative Schwarz domain decomposition algorithm. The MD and LB formulations communicate via the exchange of velocities and velocity gradients at the interface. We validate the present LB-MD model in simulations of flows of liquid argon past and through a carbon nanotube. Comparisons with existing hybrid algorithms and with reference MD solutions demonstrate the validity of the present approach.

1 Introduction

The advent of nanotechnology provides us today with nanoscale devices that can affect flow phenomena that are important for several technological applications. Examples include microfluidic channels with nanopatterned walls, biosensors embedded in aqueous environments [1, 2, 3, 4], or bluff bodies with superhydrophobic surfaces [5].

The detailed investigation of flow physics at the nanoscale has been pioneered by Koplik [6] using Molecular Dynamics (MD) models. When nanoscale devices are active parts of micro and macroscale systems, a hybrid approach is required to integrate atomistic simulations with computational methods suitable for larger scales. A number of hybrid models coupling atomistic to continuum descriptions of dense fluids have been proposed [8, 10, 9, 11, 13, 7].

O'Connell and Thompson [8] coupled an atomistic with a continuum system where the average momentum of the overlap particles is adjusted through a boundary force. Flekkøy *et al.* [9] presented a model based on direct flux exchange between atomistic and continuum regions. Hadjiconstantinou and Patera [10] proposed to decouple time scales by using the Schwarz domain decomposition method coupling an atomistic to a continuum description of a fluid. Convergence to a steady state solution is achieved through alternating iterations between steady state solutions within the atomistic and continuum subdomains. Nie *et*

al. [11, 12] employed a domain decomposition algorithm to simulate Couette flow over a nanopatterned surface, as well as a cavity flow where the singularity at the corners between static and moving walls was described atomistically. In these simulations a singular boundary force is employed in order to compensate for the elimination of periodicity in the MD system. Werder *et al.* [13] proposed an algorithm using the alternating Schwarz method to couple an MD model to an incompressible Navier-Stokes (NS) finite volume solver. They proposed a novel boundary force, based on the physical characteristics of the fluid that is being simulated. They reported on simulations of flows past a CNT and noticed average departures from reference MD simulations of the order of 4%.

Here we extend the model proposed in [13] by replacing the finite volume solver that was provided by a commercial software package (STAR-CD) by a Lattice Boltzmann (LB) method [14] solving the incompressible NS equations. The proposed extension aims to take advantage of the mesoscopic modeling inherent in LB simulations and to allow for a broader geometric flexibility than the one allowed by the Finite Volume solver. In addition, in the present work we enhance the exchange between atomistic and continuum domains by not only communicating velocities as in [13] but also velocity gradients.

The paper is organized as follows. In section 2, we describe the hybrid model by outlining the MD and LB methods and describe their coupling. Results of liquid argon flows past and through a CNT are presented in section 3. We compare the flows to the reference MD solutions and discuss the computational efficiency of the hybrid model and conclude in section 4.

2 The LB-MD model

In the present hybrid method an MD model describes the flow in the vicinity of a carbon nanotube (CNT) while a LB approach is used to simulate the behaviour of the continuum system away from the CNT.

2.1 Molecular dynamics

The atomistic region is described by MD simulations where the positions $\mathbf{r}_i = (x_i, y_i, z_i)$ and velocities $\mathbf{u}_i = (u_{x,i}, u_{y,i}, u_{z,i})$ of the particles evolve according to Newton's equations of motion

$$\frac{d}{dt}\mathbf{r}_i = \mathbf{u}_i \quad \text{and} \quad m_i \frac{d}{dt}\mathbf{u}_i = \mathbf{F}_i = - \sum_{j \neq i} \nabla U(r_{ij}) \quad (1)$$

where \mathbf{F}_i and m_i are the force and mass of particle i , and r_{ij} is the distance between the particle \mathbf{r}_i and \mathbf{r}_j . Here we consider Lennard-Jones (LJ) model of argon interacting with CNTs. The potential $U(r_{ij})$ is defined as

$$U(r_{ij}) = 4\epsilon_{AB} \left[\left(\frac{\sigma_{AB}}{r_{ij}} \right)^{12} - \left(\frac{\sigma_{AB}}{r_{ij}} \right)^6 \right] + U_b(r_w, \rho, T) \quad (2)$$

where ϵ_{AB} and σ_{AB} are energy and length parameters, A and B denote species. The LJ interaction parameters for argon-argon and argon-carbon interactions are respectively $\epsilon_{ArAr} = 0.9960 \text{ kJmol}^{-1}$, $\sigma_{ArAr} = 0.3405 \text{ nm}$, $\epsilon_{ArC} = 0.5697 \text{ kJmol}^{-1}$, $\sigma_{ArC} = 0.3395 \text{ nm}$. The term U_b is the boundary potential and accounts for the interaction of the boundary region with the surrounding medium. It is further described in [13]. The CNT is modeled as a rigid structure to facilitate the investigation of the flow of argon. All interaction potentials are truncated for distances beyond a cutoff radius $r_c = 1.0 \text{ nm}$. The equations of motion (2) are integrated using a leap-frog scheme with a time step $\delta t = 10 \text{ fs}$.

A desired velocity \mathbf{u}_d is enforced by relaxing the center of mass velocity $\bar{\mathbf{u}}_k = 1/N_k \sum_{i \in k} \mathbf{u}_i$ of the N_k particles within a cell k towards \mathbf{u}_d according to a parameter λ . The velocities \mathbf{u}_i of the particles in the cell k are updated as

$$\mathbf{u}_i = \mathbf{u}_i + \lambda(\mathbf{u}_d - \bar{\mathbf{u}}_k). \quad (3)$$

The slower the velocity relaxes towards its desired value the smaller the amount of perturbations introduced in the system. On the other hand choosing a small value of λ increases the number of iterations to reach equilibrium and thus decreases the computational efficiency. Here we choose as a relaxation parameter $\lambda = 0.1$.

2.2 Lattice Boltzmann model

The continuum hydrodynamics are described by the incompressible Navier-Stokes equations

$$\frac{\partial \mathbf{u}}{\partial t} + (\mathbf{u} \cdot \nabla) \mathbf{u} = -\nabla p / \rho + \nu \nabla^2 \mathbf{u} + \mathbf{g}, \quad (4)$$

$$\nabla \cdot \mathbf{u} = 0 \quad (5)$$

where \mathbf{u} is the fluid velocity, p the pressure, ρ the density and \mathbf{g} a body force. We use \mathbf{g} to enforce Dirichlet boundary conditions, see discussion below.

We solve the equations of motion (4) and (5) by using a Lattice Boltzmann algorithm [14]. This approach follows the evolution of particle distribution functions f_i on a d -dimensional regular lattice with z links at each lattice point \mathbf{r} . The label i denotes velocity directions and runs between 0 and z . $DdQz + 1$ is a standard lattice topology classification. The $D3Q15$ lattice we use here has the following velocity vectors \mathbf{v}_i : $(0, 0, 0)$, $(\pm 1, \pm 1, \pm 1)$, $(\pm 1, 0, 0)$, $(0, \pm 1, 0)$, $(0, 0, \pm 1)$ in lattice units.

The Lattice Boltzmann dynamics are given by

$$f_i(\mathbf{r} + \Delta t \mathbf{v}_i, t + \Delta t) = f_i(\mathbf{r}, t) + \frac{1}{\tau} (f_i^{eq}(\mathbf{r}, t) - f_i(\mathbf{r}, t)) + \Delta t g_i \quad (6)$$

where Δt is the time step of the simulation, τ the relaxation time. The equilibrium distribution function f_i^{eq} is a function of the density ρ and the fluid velocity \mathbf{u} defined as

$$\rho = \sum_{i=0}^z f_i \quad , \quad \rho \mathbf{u} = \sum_{i=0}^z f_i \mathbf{v}_i + \frac{\Delta t}{2} \mathbf{g}. \quad (7)$$

The equilibrium distribution function is chosen as

$$f_i^{eq}(\mathbf{r}, t) = w_i \rho \left(1 + \frac{\mathbf{v}_i \cdot \mathbf{u}}{c_s^2} + \frac{(\mathbf{v}_i \cdot \mathbf{u})^2}{2c_s^4} - \frac{\mathbf{u}^2}{2c_s^2} \right) \quad (8)$$

where $c_s = 1/\sqrt{3}$ is the speed of sound and w_i are weights chosen as $w_0 = 4/9$, $w_i = 1/9$ for $i = 1 - 6$ and $w_i = 1/72$ for $i = 7 - 14$. The forcing term is defined as [15]

$$g_i = \left(1 - \frac{1}{2\tau} \right) w_i \rho \left(\frac{\mathbf{v}_i - \mathbf{u}_i}{c_s^2} + \frac{(\mathbf{v}_i \cdot \mathbf{u}_i)}{c_s^4} \mathbf{v}_i \right) \cdot \mathbf{g}. \quad (9)$$

Performing a Chapman-Enskog expansion on the LB dynamics [16] shows that equations (4) and (5) are recovered with a kinematic viscosity expressed as

$$\nu = \frac{(\Delta \mathbf{r})^2}{\Delta t} \frac{1}{3} \left(\tau - \frac{1}{2} \right) \quad (10)$$

where $\Delta \mathbf{r}$ is the lattice spacing.

We enforce Dirichlet boundary conditions using a local forcing term \mathbf{g} . The governing equation Equation (4) is rewritten as

$$\frac{\partial \mathbf{u}}{\partial t} = \frac{\mathbf{u}^*(\mathbf{r}, t + \Delta t) - \mathbf{u}(\mathbf{r}, t)}{\Delta t} = -(\mathbf{u} \cdot \nabla) \mathbf{u} - \nabla p + \nu \nabla^2 \mathbf{u} = RHS \quad (11)$$

where \mathbf{u}^* is the velocity at time $t + \Delta t$ with no forcing term considered. Including a forcing term leads to

$$\frac{\mathbf{u}^d(\mathbf{r}, t + \Delta t) - \mathbf{u}(\mathbf{r}, t)}{\Delta t} = RHS + \mathbf{g}(\mathbf{r}, t) \quad (12)$$

where \mathbf{u}^d is the desired velocity. Subtracting equations (11) from (12) leads to an expression for the forcing term

$$\mathbf{g}(\mathbf{r}, t) = \frac{\mathbf{u}^d(\mathbf{r}, t + \Delta t) - \mathbf{u}^*(\mathbf{r}, t + \Delta t)}{\Delta t}. \quad (13)$$

It is worth noting that evaluating \mathbf{u}^* within an LB method consists only of performing a streaming step. Indeed by construction of the equilibrium distribution function ($\rho \mathbf{u} = \sum f_i^{eq} \mathbf{v}_i$, see [16] for details), the second term of the right hand side of equation (6) does not change the velocity \mathbf{u} .

2.3 Hybrid model

We use a domain decomposition algorithm to couple an MD description of a dense fluid with an LB model solving the incompressible NS equations. The computational domain is decomposed into two overlapping regions of an LB domain and an MD subdomain. Fig. 1 shows the Schwarz decomposition used to converge to a steady state solution by alternating iterations between steady state solutions in the LB domain and MD subdomain.

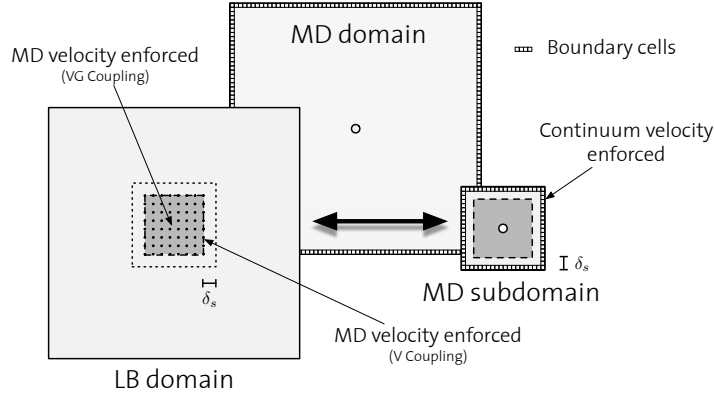


Figure 1: Domain decomposition. The dark gray area is computed within the MD subdomain and (VGC) enforced within the LB domain or (VC) only enforced along a strip depicted by the dashed square. Converged solution is obtained by alternating iterations in the LB and MD domains.

A Schwarz iteration t_c consists of computing the continuum velocity field $\mathbf{u}_c(t_c)$ with boundary conditions set by the previous atomistic cycle $\mathbf{u}_a(t_c-1)$ and an external boundary condition that depends on the system considered. Then, $\mathbf{u}_c(t_c)$ is used to set the boundary condition for computing $\mathbf{u}_a(t_c)$.

MD velocities are sampled in cells of same size as in the LB domain and are enforced on the continuum according to two coupling methods using equation (13). The first approach corresponds to the one used by Werder *et al.* and is to impose MD velocities within a one cell wide strip located at a distance δ_s of the MD subdomain, see fig. 1. This velocity coupling (VC) approach does not enforce velocity gradients implying that the geometry of the system and the external boundary conditions dictate whether the hybrid solution evolve into a good approximation of the reference solution. To alleviate this issue we propose an enriched coupling method which enforces velocities, and implicitly velocity gradients (VGC) by imposing MD velocities on every common cell except within a strip of width δ_s close to the boundary (see fig. 1). We shall observe below that using the VGC approach leads to closer match with MD reference solutions than when using the VC method.

We use the algorithm proposed by Werder *et al.* [13] to impose non-periodic boundary conditions (NPBC) on the MD system. Details of the algorithm can be found in [13].

3 Results

We first consider the flow past a CNT embedded normal to the flow direction in order to compare our results with [13]. We then discuss the flow through a short CNT embedded parallel to the flow direction.

3.1 Flow past a nanotube

We apply the hybrid LB-MD algorithm to the case of the flow of argon around a CNT centered along the z-axis within a $30 \times 30 \times 4.254 \text{ nm}^3$ domain Ω . The CNT is of chirality $(16, 0)$ with a radius of $r = 0.625 \text{ nm}$. We choose the density of argon $\rho_{Ar} = 1008 \text{ kgm}^{-3}$ and the temperature $T = 215 \text{ K}$. This corresponds to the dimensionless state point $(T^*, \rho^*) = (1.8, 0.6)$ where $T^* = k_B T \epsilon_{ArAr}^{-1} \mathcal{A}$ and $\rho^* = \rho \sigma_{ArAr}^3 m_{Ar}^{-1} \mathcal{A}$. We let k_B be the Boltzmann constant, $m_{Ar} = 0.03994 \text{ kgmol}^{-1}$ the atomic mass of argon, and \mathcal{A} Avogadro's number.

The MD subdomain size is $10 \times 10 \times 4.254 \text{ nm}^3$ centered around the CNT which is subdivided into $20 \times 20 \times 1$ sampling cells where 6465 argon atoms are initially equilibrated for 0.2 ns. The width of the strip around the boundary on which both MD and LB are simulated is $\delta_s = 2.5 \text{ nm}$.

We consider an LB domain of size $60 \times 60 \times 1$ covering the entire domain where lattice nodes are centered on the corresponding MD sampling cells. The viscosity of the LJ fluid is a parameter of the LB model and set to $\nu = 0.745 \cdot 10^{-7} \text{ m}^2\text{s}^{-1}$ [17]. We have performed a sensitivity analysis by increasing and decreasing the viscosity by 5% and found it to be a robust parameter with respect to accuracy. Dirichlet boundary conditions $u_\infty = u_x = 100 \text{ ms}^{-1}$ are imposed at the inlet $x = 0 \text{ nm}$ and outlet $x = 30 \text{ nm}$. This high velocity is chosen to reduce the number of sampling iterations. The temperature is controlled by using a Berendsen thermostat [18] with a time constant $\tau_T = 0.1 \text{ ps}$. We apply it cell-wise in all directions in the boundary cells where the velocity is prescribed and only in the z-direction in other cells. The hybrid model is run for 100 cycles which consists of running the LB simulation for 7 ns (15000 iterations) followed by an MD step equilibrating for 0.2 ns (20000 iterations) and sampling for $t_s = 0.4 \text{ ns}$. We discuss below how t_s affects the convergence of the results.

Fig. 2 shows a comparison between hybrid converged solutions and an MD reference solution over the entire domain. The latter involves 58198 argon atoms and the temperature is controlled as in the MD subdomain. The reference MD velocity field is sampled over 20 ns. A qualitative match with the reference MD solution is obtained when using the VC approach. The match between the hybrid solution and the reference MD solution becomes quantitative when using the VGC method. This is due to the fact that velocity gradients are not let free but implicitly imposed. A consequence of this is that discrepancies in the wake and on the sides of the CNT that appears when using the VC approach, and also reported in [13], are not observed when using the VGC method.

Fig. 3 shows the evolution of the norm of the velocity along the $y = 15 \text{ nm}$ and $x = 15 \text{ nm}$ plane. The system starts from a constant initial condition $u_x = u_\infty = 100 \text{ ms}^{-1}$. This unphysical state leads to the formation of high velocity regions around the CNT. They then slowly spread out on the sides of the tube and increase the side velocity. Considering the VGC approach, we observe that the velocity upstream and downstream adjusts smoothly to the reference solution. The situation is different when employing the VG method. Indeed the hybrid velocity profiles show deviations from the MD reference solution especially downstream the CNT. It is worth noting that we get identical results

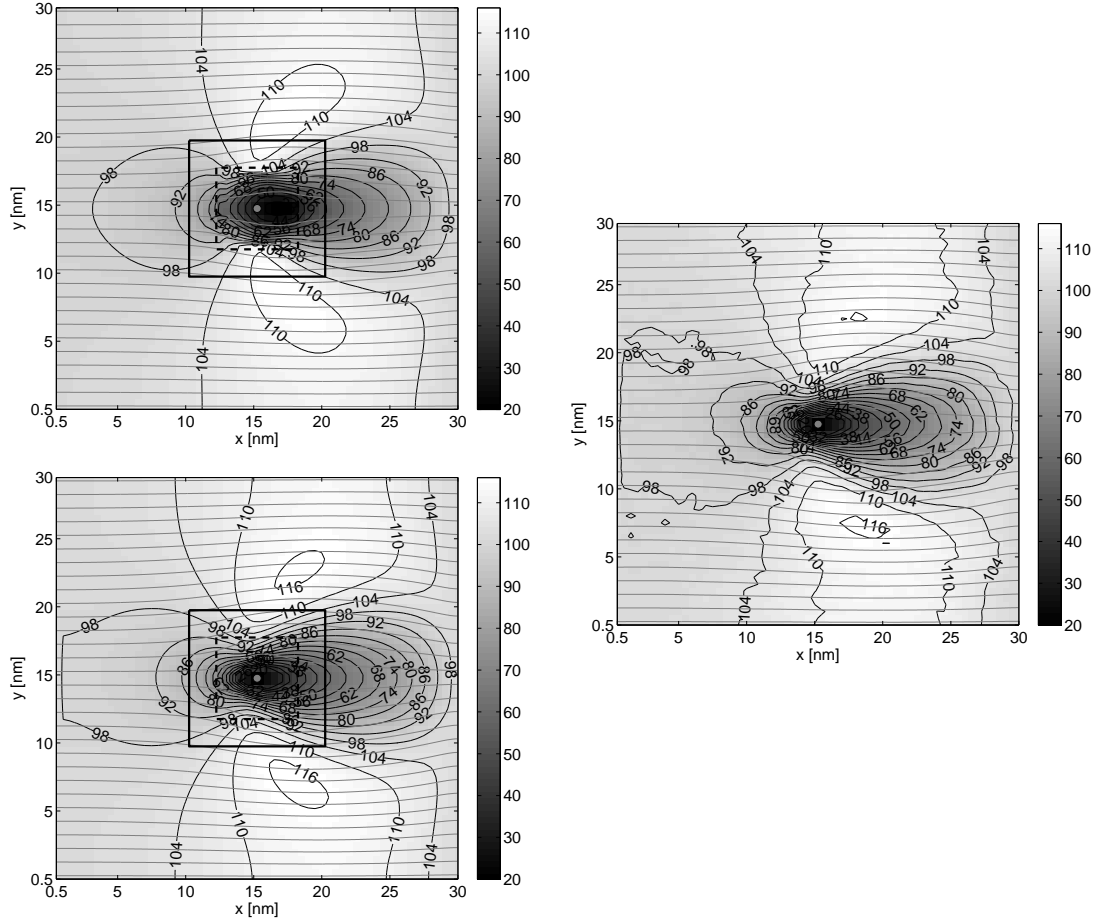


Figure 2: (left) Converged hybrid and (right) reference MD solutions of a flow past a CNT. (top) Velocities and (bottom) velocities and velocity gradients are enforced. The colorscale and contour lines depict the norm of the velocity expressed in ms^{-1} . Gray lines are streamlines. The thick squares represent (solid) the boundary of the MD subdomain and (dashed) the boundary of the overlapping region.

when initializing the system with initial conditions closer to the steady solution.

In agreement with [19], we observe that argon flow past a CNT normal to the flow results in a vanishing velocity at the surface of the CNT. In this particular configuration, the velocity boundary condition around the tube can therefore be approximated by a no-slip condition allowing us to solve the NS equations. Fig. 3 shows LB velocity profiles where the CNT is modeled off-lattice using an Immersed Boundary technique [20]. We will see however that this approximation is not applicable when we consider a CNT with a different orientation.

We quantify the convergence towards the reference MD solution by defining an error e^j between the hybrid solution at cycle j and the reference MD solution as

$$e^j = \frac{1}{N} \sum_{k \in \Omega} \frac{|\mathbf{u}_k^j - \mathbf{u}_{k,MD}|}{u_\infty} \quad (14)$$

where N is the number of cells in Ω , \mathbf{u}_k^j and $\mathbf{u}_{k,MD}$ are respectively the hybrid and reference MD velocities at cycle j in the cell k .

Fig. 4 shows the time evolution of the error which rapidly decays during the first 10 cycles. The error then fluctuates around an average value which is a function of t_s . Considering the VGC approach, we measure an average error between cycle 50 and 100 of 1.3% for $t_s = 0.4$ ns and $t_s = 0.8$ ns and an average error of 1.9% for $t_s = 0.2$ ns. We observe in fig. 4 that considering short t_s leads to undesirable fluctuations whereas long t_s decreases the computational efficiency of the model. An optimum is found to be $t_s = 0.4$ ns assumed hereafter if not otherwise specified. Fig. 4 also shows the time evolution error when using the VC method. The average error between cycle 50 and 100 is of 3.8% and is comparable to the error evolution reported in [13].

The point-wise error between the hybrid and the reference MD solutions is depicted in fig. 4. Using the VGC technique leads to a localized and maximum 3.9% error region showing only on one side of the CNT. Everywhere else the error is up to 2.5%. The error is higher when using the VC approach where we observe a large error of 40% close to the CNT and up to 12% in the wake.

The supercritical state point $(T^*, \rho^*) = (1.8, 0.6)$ is associated with less structural correlations than in a liquid state. In order to assess their effect on the convergence we have considered the liquid state point $(131K, 1361 \text{ kgm}^{-3}) = (1.09, 0.81)$ related to the kinematic viscosity $\nu = 1.42 \cdot 10^{-7} \text{ m}^2\text{s}^{-1}$ [17]. For similar parameters as for the state points $(1.8, 0.6)$, we measure an error of 2.0% between the hybrid solution and the associated reference MD solution. The error is slightly higher than the one obtained in the supercritical state and indicates that the LB-MD model can also be applied when considering liquid states.

3.2 Flow through a nanotube

We now consider the flow through a CNT driven driven by a constant velocity $u_x = 100 \text{ ms}^{-1}$ enforced at $x = 0$ nm and $x = 28$. The CNT is centered along the x-axis in a domain

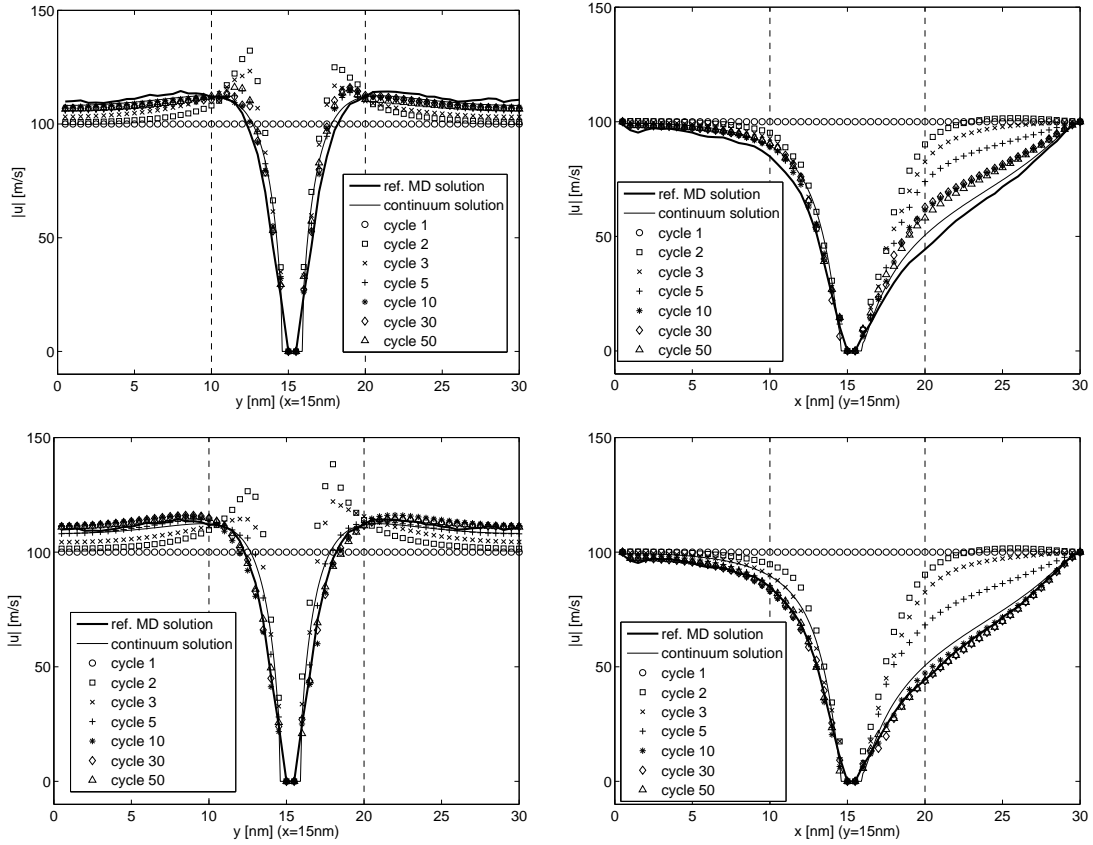


Figure 3: Evolution of the hybrid profiles of the norm of the velocity in the planes located (left) at $x = 15$ nm and (right) at $y = 15$ nm. (top) Velocities and (bottom) velocities and velocity gradients are enforced. The solid thick line is the reference MD solution whereas the solid line is the continuum solution where no-slip boundary condition is considered around the CNT. Hybrid solutions are plotted after various number of cycles. Dashed lines represent the boundaries of the MD subdomain.

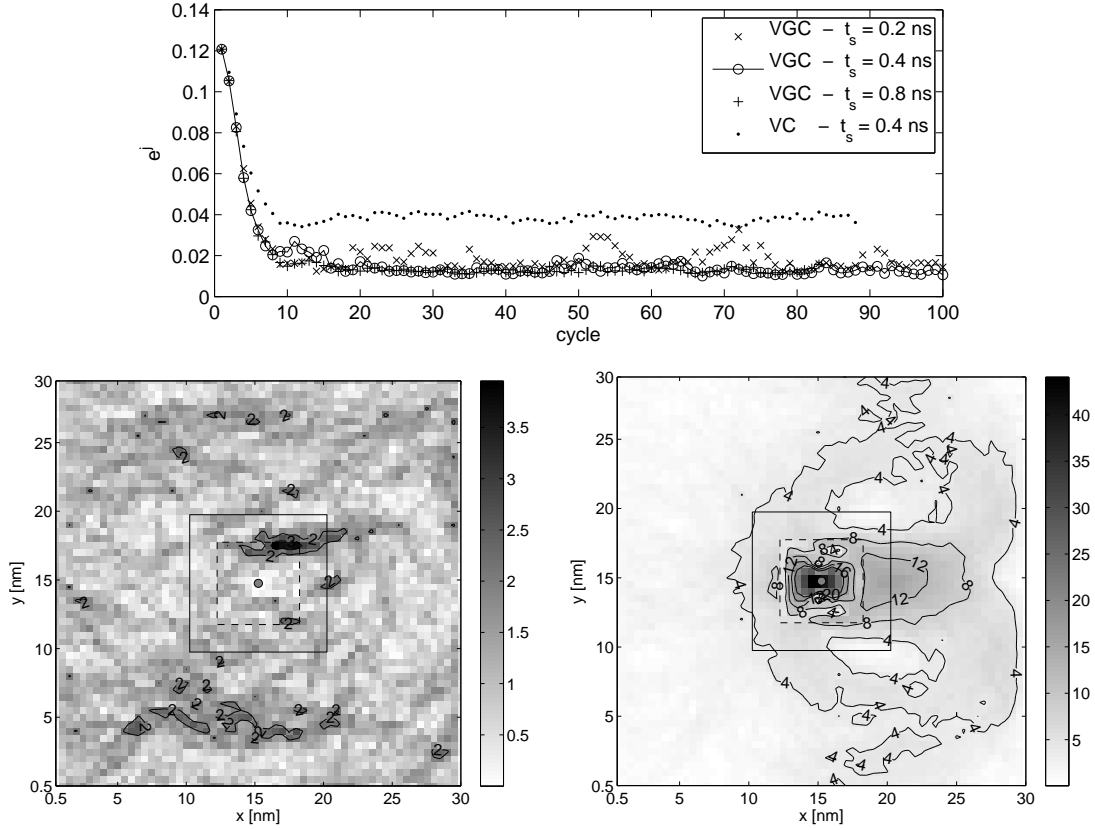


Figure 4: (top) Evolution of the error e^j between the hybrid solution and the reference MD solution. Different sampling time t_s and coupling techniques are considered. (bottom) Point-wise error according to equation (14) shown in percentage and averaged between cycle 50 and 100. The sampling time $t_s = 0.4$ ns. (left) The VGC and (right) the VC techniques are used.

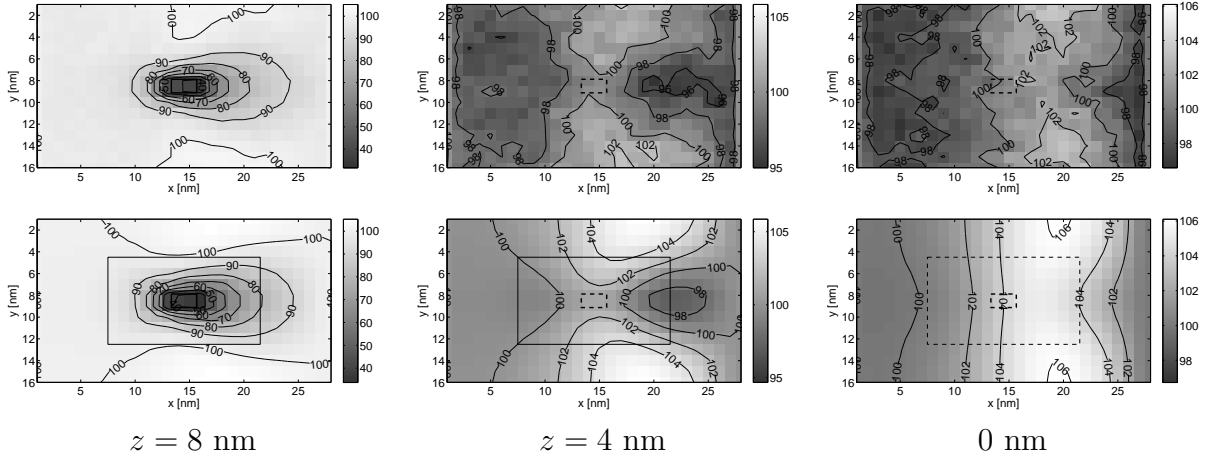


Figure 5: Reference MD (top) and hybrid (bottom) solutions of the flow through a CNT driven by a constant velocity $u_x = 100 \text{ ms}^{-1}$ enforced at $x = 0 \text{ nm}$ and $x = 28 \text{ nm}$. The norm of the velocity is plotted. Each column corresponds to a different $x - y$ plane at $z = 8, 4$ and 0 nm . Contour lines are plotted and expressed in ms^{-1} . Bold and thin rectangles depict the CNT and the MD subdomain respectively.

of size $28 \times 16 \times 16 \text{ nm}^3$ and it is of chirality $(16, 0)$ with a length $l = 2.34 \text{ nm}$. We choose the dimensionless state point $(T^*, \rho^*) = (1.8, 0.6)$.

The MD subdomain size is $14 \times 10 \times 10 \text{ nm}^3$ centered around the CNT and is subdivided into $14 \times 10 \times 10$ sampling cells. 21278 argon atoms are initially equilibrated for 0.2 ns and $\delta_s = 3 \text{ nm}$. The temperature is regulated by applying a Berendsen thermostat cell-wise in every direction within the boundary cells. We consider a $28 \times 16 \times 16 \text{ LB}$ domain covering the entire domain where lattice nodes are centered in corresponding sampling cells. MD and LB domains are coupled via the VGC approach. The hybrid model is ran for 50 cycles consisting of running the LB simulation for 13.4 ns (15000 iterations) followed by an MD step equilibrated for 0.2 ns and sampled for $t_s = 0.4 \text{ ns}$.

Fig. 5 shows a comparison between the hybrid and the reference MD solution. The latter consists of 108943 argon atoms sampled for 20 ns where thermal boundary conditions are as in the MD subdomain. There is an overall good quantitative agreement between the solutions. We observe regions above and under the CNT where the hybrid velocity is slightly faster than in the reference MD solution. The difference is at most 4%. We quantify the overall agreement by measuring average errors following equation (14) over different regions and during the last 30 cycles and obtain a global error $e_g = 2.6\%$ over the whole domain and a local error $e_l = 2.1\%$ in the tube.

The rather small diameter of the CNT leads to a higher argon density within the tube. We measure a 7% increase that can not be described by the incompressible NS equations. This issue could however be alleviated by considering a compressible LB model [21].

In this conformation, the velocities around the CNT are non-zero. The corresponding

continuum velocity boundary condition is unknown and a function of the system parameters [19]. A continuum solution approximating the reference solution is therefore unfeasible.

The computational efficiency of the LB-MD model is estimated by comparing the time needed to compute one iteration of the reference and hybrid solution, respectively. We measure $t_{ref} = 0.56$ s and $t_{hyb} = 0.08$ s in the case of the flow past a CNT. The hybrid solution is computed $R = 0.56/0.08 = 7$ times faster than the reference solution. We get a ratio $R = 1.04/0.43 = 2.4$ in the case of a flow through a CNT. Ratios R are of the same order as the volume ratio between the MD domain and subdomain. Small systems have been chosen here in order to compare hybrid to reference solutions. Considering larger systems would exhibit much higher ratios. For example, nanodevices ($\propto 10^3$ nm³) embedded in microscale systems ($\propto 1$ μ m³) would lead to ratios of the order of 10^6 .

4 Conclusion

We have presented a hybrid model coupling a Lattice Boltzmann solution of the incompressible Navier-Stokes equations to a Molecular Dynamics Simulation of a dense fluid, using a Schwarz domain decomposition technique. The two descriptions are coupled via an exchange of velocities (VC) or velocity gradients (VGC). The applicability of the method was demonstrated in flows of liquid argon past Carbon Nanotubes normal and aligned with the flow velocity.

We have first computed the flow past a CNT with an axis normal to the flow velocity. Using the VGC approach we observed quantitative agreement between the hybrid and the reference MD solutions with an average error of 1.3% that provides an improvement over previously reported results [13] for the same configuration. We attribute this improvement to the fact that we enforce velocity within a region rather than along a strip implying that velocity gradients and in turn shear forces are implicitly exchanged between the two descriptions. We also show that the velocity vanishes around the tube in this conformation making a continuum solution a good approximation of the reference solution. This is not the case however when considering the flow through a CNT. The transport of argon in the CNT is captured within 2.1% with our LB-MD model. To the best of our knowledge, this is the first time that fully 3D hybrid simulations have been reported in the literature.

In addition of being a tool to help investigating multi-scale physics by considerably reducing an otherwise prohibitive computational time, this approach largely extends the applicability of LB models by providing us with fully microscopic boundary conditions.

Acknowledgment

We wish to thank P.G. Gonnet for many helpful technical discussions.

References

- [1] R.J. Chen, S. Bangsaruntip, K.A. Drouvalakis, N.W.S. Kam, M. Shim, Y.M. Li, W. Kim, P.J. Utz, and H.J. Dai. Noncovalent functionalization of carbon nanotubes for highly specific electronic biosensors. *Proc. Natl. Acad. Sci. USA*, 100:4984, 2003.
- [2] J. Li, H.T. Ng, A. Cassell, W. Fan, H. Chen, Q. Ye, J. Koehne, J. Han, and M. Meyyappan. Carbon nanotube nanoelectrode array for ultrasensitive DNA detection. *Nano Letters*, 3:597, 2003.
- [3] Y. Lin, S. Taylor, H. Li, K.A. Fernando Shiral, L. Qu, W. Wang, L. Gu, B. Zhou, and Y.-P. Sun. Advances toward bioapplications of carbon nanotubes. *J. Mater. Chem.*, 14:527, 2004.
- [4] M. Zheng, A. Jagota, E.D. Semke, B.A. Diner, R.S. McLean, S.R. Lustig, R.E. Richardson, and N.G. Tassi. DNA-assisted dispersion and separation of carbon nanotubes. *Nature Mat.*, 2:338, 2003.
- [5] K. Watanabe, T. Takayama S. Ogata, and S. Isozaki. Flow between two coaxial rotating cylinders with a highly water-repellent wall. *AIChE J.*, 49:1956, 2003.
- [6] J. Koplik and J.R. Banavar. Continuum deductions from molecular hydrodynamics. *Annu. Rev. Fluid Mech.*, 27:257, 1995.
- [7] P. Koumoutsakos. Multiscale flow simulations using particles. *Ann. Rev. Fluid Mech.*, 37:457, 2005.
- [8] S.T. O’Connell and P.A. Thompson. Molecular dynamics-continuum hybrid computations: A tool for studying complex fluid flow. *Phys. Rev. E*, 52:R5792, 1995.
- [9] E.G. Flekkøy, G. Wagner, and J. Feder. Hybrid model for combined particle and continuum dynamics. *Europhys. Lett.*, 52:271, 2000.
- [10] N.G. Hadjiconstantinou and A.T. Patera. Heterogeneous atomistic-continuum representations fo dense fluid systems. *Int. J. Modern Phys. C*, 8:967, 1997.
- [11] X.B. Nie, S.Y. Chen, W.N. E, and M.O. Robbins. A continuum and molecular dynamics hybrid method for micro- and nano-fluid flow. *J. Fluid Mech.*, 500:55, 2004.
- [12] X.B. Nie, S.Y. Chen, and M.O. Robbins. Hybrid continuum-atomistic simulation of singular corner flow. *Phys. Fluids*, 16:3579, 2004.
- [13] T. Werder, J.H. Walther, and P. Koumoutsakos. Hybrid atomistic-continuum method for the simulation of dense fluid flows. *J. Comp. Phys.*, 205:373, 2005.
- [14] S. Succi. *The Lattice Boltzmann Equation, For Fluid Dynamics and Beyond*. Oxford University Press, 2001.

- [15] Z. Guo, C. Zheng, and B. Shi. Discrete lattice effects on the forcing term in the lattice Boltzmann method. *Phys. Rev. E*, 65:046308, 2002.
- [16] B. Chopard and M. Droz. *Cellular Automata Modeling of Physical Systems*. Cambridge University Press, 1998.
- [17] K. Meier, A. Laesecke, and S. Kabelac. Transport coefficients of the Lennard-Jones model fluid. I. Viscosity. *J. Chem. Phys.*, 121:3671, 2004.
- [18] H.J.C. Berendsen, J.P.M. Postma, W.F. van Gunsteren, A. DiNola, and J.R. Haak. Molecular dynamics with coupling to an external bath. *J. Chem. Phys.*, 81:3684, 1984.
- [19] J.H. Walther, T. Werder, R.L. Jaffe, and P. Koumoutsakos. Hydrodynamic properties of carbon nanotubes. *Phys. Rev. E*, 69:062201, 2004.
- [20] A. Dupuis and P. Koumoutsakos. Immersed boundary method in lattice Boltzmann flows. In preparation.
- [21] A.J. Briant, A.J. Wagner, and J.M. Yeomans. Lattice Boltzmann simulations of contact line motion. I. Liquid-gas systems. *Phys. Rev. E*, 69:031602, 2004.